Check for updates

CMIP5 model simulations of warm Arctic-cold Eurasia pattern in winter surface air temperature anomalies

Sai Wang[1,2] · Debashis Nath[1] · Wen Chen[1,2] · Tianjiao Ma[1]

Abstract

The second empirical orthogonal function mode (EOF2) of winter surface air temperature (SAT) over 0°–180° E, 40°–90° N during 1979–2005 is defined as warm Arctic-cold Eurasia (WACE) pattern. The present study evaluates the performance of 25 Coupled Model Inter-comparison Project Phase 5 (CMIP5) models in simulating the WACE pattern based on historical runs. There exist large inter-model spreads in the simulation of the WACE pattern. Analyses show that the ability of a CMIP5 model in capturing the WACE pattern is connected with the model's performance in representing the observed atmospheric circulation anomalies related to the winter sea ice concentration (SIC) variation over Barents–Kara Seas. Sea ice loss over Barents–Kara Seas can induce significant positive geopotential height anomalies over Arctic region and negative geopotential height anomalies around the Baikal Lake, resulting in warm anomalies over Barents–Kara Seas and cold anomalies over Eurasia. Further analysis shows that CMIP5 model's performance in representing the SAT anomalies related to the WACE pattern is partly due to simulation of the amplitude of winter SIC variability over Barents–Kara Seas. Larger standard deviations of winter SIC over Barents–Kara Seas can instigate stationary wave-train more easily, which further induces the SAT anomalies.

Keywords Winter · Warm Arctic-cold Eurasia · Atmospheric circulation anomalies · Sea ice · CMIP5

1 Introduction

Despite an increasing trend in the global annual mean temperature, in the recent years apparent cooling trends are observed over central Siberia during the boreal winter months (Cohen et al. 2012a, b). It is accompanied with the recovery of Siberian High (Jeong et al. 2011) and re-amplification of the East Asian winter monsoon since the mid-2000s (Wang and Chen 2013). Moreover, in the past decade severe winters have occurred frequently over the Eurasian continents (Liu et al. 2012; Tang et al. 2013; Mori et al. 2014). Simultaneously, Arctic has experienced rapid warming and sea-ice loss in the past few decades (Polyakov et al. 2002; Johannessen et al. 2004; Screen and Simmonds 2010a,

b; Serreze and Barry 2011; Screen et al. 2012). The pattern of this Northern Hemispheric (NH) temperature signal is often referred as "Warm Arctic, Cold Continents" (Overland et al. 2010; Cohen et al. 2013, 2014).

In some recent papers, it is a topic of great debate whether the Eurasian cooling is caused by the Arctic sea ice loss and Arctic warming or not (Francis and Vavrus 2012; Liu et al. 2012; Tang et al. 2013; Sun et al. 2016; Liang et al. 2020; Warner et al. 2019). For example, Sun et al. (2016) has attributed the Eurasian cooling to the natural variability or the pre-existing atmospheric patterns. However, it has been speculated that the occurrence of cold SAT anomalies over Eurasia is due to the impact of Arctic sea ice loss and warming based on the observed coincidence of trends or statistical correlations (Francis and Vavrus 2012; Hopsch et al. 2012; Inoue et al. 2012; Liu et al. 2012; Tang et al. 2013). Some model simulations also find a connection between Arctic sea ice loss and cooling over midlatitude continents (Honda et al. 2009; Liu et al. 2012; Mori et al. 2014; Kug et al. 2015). Some studies indicated that cold Eurasian winters could have been instigated by Arctic sea-ice decline through excitation of negative Arctic Oscillation (AO)-like structure circulation

✉ Debashis Nath
debashis@mail.iap.ac.cn

[1] Center for Monsoon System Research, Institute of Atmospheric Physics, Chinese Academy of Sciences, Beijing, China

[2] College of Earth and Planetary Sciences, University of Chinese Academy of Sciences, Beijing, China

anomalies (Honda et al. 2009; Liu et al. 2012; Screen et al. 2013; Peings and Magnusdottir 2014). Mori et al. (2014) has extracted the two leading modes governing winter surface air temperature (SAT) anomalies over Eurasia by applying empirical orthogonal function (EOF) analysis to winter surface air temperature (SAT) over 0°–180° E, 20°–90° N. The first mode (EOF1) represents a pattern of uniform warming over the entire Eurasian continent and associated principal component (PC1) is highly correlated with the AO index. The second mode (EOF2) is defined as warm Arctic-cold Eurasia (WACE) pattern, which is characterized by warm anomalies over Barents–Kara Seas and cold anomalies over central Eurasia at its positive phase. It is found that this pattern represents SAT variation associated with the wintertime sea ice variation in the Barents–Kara Seas and is likely to be more responsible for the recent increase in the frequency of severe winters than AO (Mori et al. 2014).

Climate models are widely applied to understand and improve the predictions of climate systems over the globe. The Coupled Model Inter-comparison Project Phase 5 (CMIP5) is an efficient data source to study global climate change (Taylor et al. 2012). Some previous studies have been carried out to evaluate the capacity of CMIP5 models in simulating the Eurasian SAT variability in winter (Miao et al. 2014; Guo et al. 2016; Xu et al. 2016). Miao et al. (2014) assessed the performance of the CMIP5 models in simulating the intra-annual, annual and decadal temperature over Northern Eurasia from 1901 to 2005. Guo et al. (2016) evaluated the capacity of CMIP5 models in capturing the dominant modes of winter SAT variations over China. Xu et al. (2016) investigated change in the first two EOF modes of boreal winter SAT variations over East Asia (0°–60° N and 100°–140° E) under global warming. According to the recently published review article by Cohen et al (2020), not all CMIP5 models support the link between Arctic warming and severe winter weather over mid-latitude Eurasia, implying their diverse ability in capturing the WACE pattern. Therefore, the present study will investigate the ability of the CMIP5 coupled models in capturing the present-day (1979–2005) WACE pattern. Furthermore, we will also find out the key factors responsible for CMIP5 model's performance in reproducing the WACE pattern. The remainder of the paper is organized as follow: Sect. 2 describes the reanalysis datasets, CMIP5 models and the analysis methods. Section 3 shows the assessments of the present-day climatology pattern and interannual variability of winter SAT. The performance of the CMIP5 models in simulating the WACE pattern is examined in Sect. 4. A brief summary is provided in Sect. 5. The discussion is finally given in Sect. 6.

2 Data and methods

2.1 Data

The atmospheric variables employed in this study were obtained from ERA-Interim reanalysis with a horizontal resolution of $2.5° \times 2.5°$, which is available from 1 January 1979 to 31 August 2019 (Dee et al. 2011). The ERA-Interim reanalysis is widely applied for investigating the Arctic climate variability (Wang et al.2019; Park et al. 2015; Mori et al. 2014) due to its good representation of Arctic climate (Lindsay et al. 2014; Zygmuntowska et al. 2012). The sea ice concentration (SIC) data were obtained from Met Office Hadley Centre for Climate Prediction and Research, which is available from 1870 on a horizontal resolution of $1° \times 1°$ (Rayner et al. 2003). For convenience, the observational and reanalysis datasets are all defined as "observations" (OBS) in remaining of the study. This study uses outputs of 25 climate models from the CMIP5. Table 1 presents brief descriptions of these CMIP5 models, including their horizontal resolutions, institutions, and model names. Since several CMIP5 models only have one realization of the historical experiments, to maintain consistency the first standard run from each model has been analyzed in this study. In addition, the period from 1979 to 2005 of the historical experiment is employed to compare against the observations. The results obtained in this study would not change much based upon the base period selection. The atmospheric variables derived from the CMIP5 historical are converted to a standard 2.5° latitude–longitude grid, and SIC from model outputs are converted to a standard 1° latitude–longitude grid.

2.2 Methods

In this study, the multimodel ensemble (MME) is calculated by averaging the variables over all the models with equal weighting. The Taylor diagram is used to analyze the performance of the CMIP5 models in simulating the spatial pattern of any variable in terms of the spatial correlation coefficient, root mean square error, and ratio of their standard deviation (STD) (Taylor 2001). Different from Mori et al. (2014), the present study focuses on analyzing the interannual variations. Therefore, except for the analyses of climatology and standard deviation of winter SAT, all the data are linearly detrended over the period 1979–2005, both for observations and CMIP5 models. Based on Mori et al. (2014), an empirical orthogonal function (EOF) analysis used to extract the WACE pattern. Prior to the EOF analysis, the detrended DJF-mean SAT anomalies are weighted by cosine of latitude so that the

Table 1 Information of the CMIP5 models used in this study

| Model name	Modeling center	Resolution (lat, lon)
ACCESS1-0	Commonwealth Scientific and Industrial Research Organization and Bureau of Meteorology, Australia	144×192
ACCESS1-3	Commonwealth Scientific and Industrial Research Organization and Bureau of Meteorology, Australia	64×128
bcc-csm1-1-m	Beijing Climate Center, China Meteorological Administration, China	160×320
CanESM2*	Canadian Centre for Climate Modeling and Analysis, Victoria, BC, Canada	192×288
CCSM4	National Center for Atmospheric Research (NCAR) Boulder, CO, USA	192×288
CESM1-BGC	Community Earth System Model contributors	192×288
CESM1-CAM5	Community Earth System Model contributors	96×144
CESM1-WACCM*	Community Earth System Model contributors	240×480
CMCC-CM	Centro Euro-Mediterraneo per I Cambiamenti Climatici	96×193
CSIRO-Mk3-6-0	Commonwealth Scientific and Industrial Research Organisation in collaboration with the Queensland Climate Change Centre of Excellence, Australia	60×128
FGOALS-g2	Institute of Atmospheric Physics, Chinese Academy of Sciences, China	108×128
FGOALS-s2	Institute of Atmospheric Physics, Chinese Academy of Sciences, China	64×128
FIO-ESM	First Institute of Oceanography, State Oceanic Administration, China	90×144
GFDL-CM3*	NOAA, Geophysical Fluid Dynamics Laboratory	90×144
GISS-E2-H-CC	NASA Goddard Institute for Space Studies	90×144
GISS-E2-R-CC	NASA Goddard Institute for Space Studies	120×180
inmcm4	Institute for Numerical Mathematics, Russia	143×144
IPSL-CM5A-MR	Institute Pierre Simon Laplace, Paris, France	96×96
IPSL-CM5B-LR	Institute Pierre Simon Laplace, Paris, France	64×128
MIROC-ESM	Japan Agency for Marine-Earth Science and Technology, Atmosphere and Ocean Research Institute, and National Institute for Environmental Studies, Japan	320×640
MIROC4h	Atmosphere and Ocean Research Institute (University of Tokyo), National Institute for Environmental Studies, and Japan Agency for Marine-Earth Science and Technology	96×192
MPI-ESM-LR	Max Planck Institute for Meteorology, Germany	96×192
MPI-ESM-P	Max Planck Institute for Meteorology, Germany	96×192
MRI-CGCM3*	Meteorological Research Institute, Japan	160×320
NorESM1-M*	Norwegian Climate Centre, Norway	96×144

Models masked with an asterisk are the high correlation (HC) models, whiles those in bold text are the low correlation (LC) models

individual grid points have equal weightage (North et al. 1982). Then the EOF analysis of DJF mean SAT anomalies was conducted within the domain 0°–180° E and 40°–90° N by computing eigenvalues and eigenfunctions of the covariance matrix. The sum of explained variation by the two leading EOFs obtained from ERA-interim reanalysis datasets is ~ 57.83%. The present study estimates the confidence level according to the two-tailed Student's t test.

3 Climatology and standard deviation

In this section, we first evaluate the capability of the CMIP5 models in reproducing the climatology and the standard deviation of winter SAT during the period of 1979–2005. Figure 1 displays the observations (OBS), multi-model ensemble mean (MME), i.e. the mean of all available 25 models from Table 1 and the difference between MME and

OBS for the climatology and standard deviation of winter (December–January–February; DJF) SAT. In OBS, relatively low climatological winter SAT can be observed north of about 40° N, with the lowest values located over the north Siberia and the Far East over Russia (Fig. 1a). Large standard deviation of winter SAT appears over the Barents–Kara Seas region and northern Siberia (Fig. 1b). In general, the MME captures the spatial distribution of climatological winter SAT considerably well. In particular, the MME generally captures the location of the cold center over the north Siberia and the Far East over Russia (Fig. 1b). However, MME tends to underestimate the climatological winter SAT in Arctic, especially over Barents Sea, and overestimate over and around the Caspian Sea and eastern part of Russia, which can be seen more clearly in the difference map (Fig. 1c) between the observed and simulated climatological winter SAT. Difference maps show that the climatological winter SAT over eastern part of Russia is overestimated by
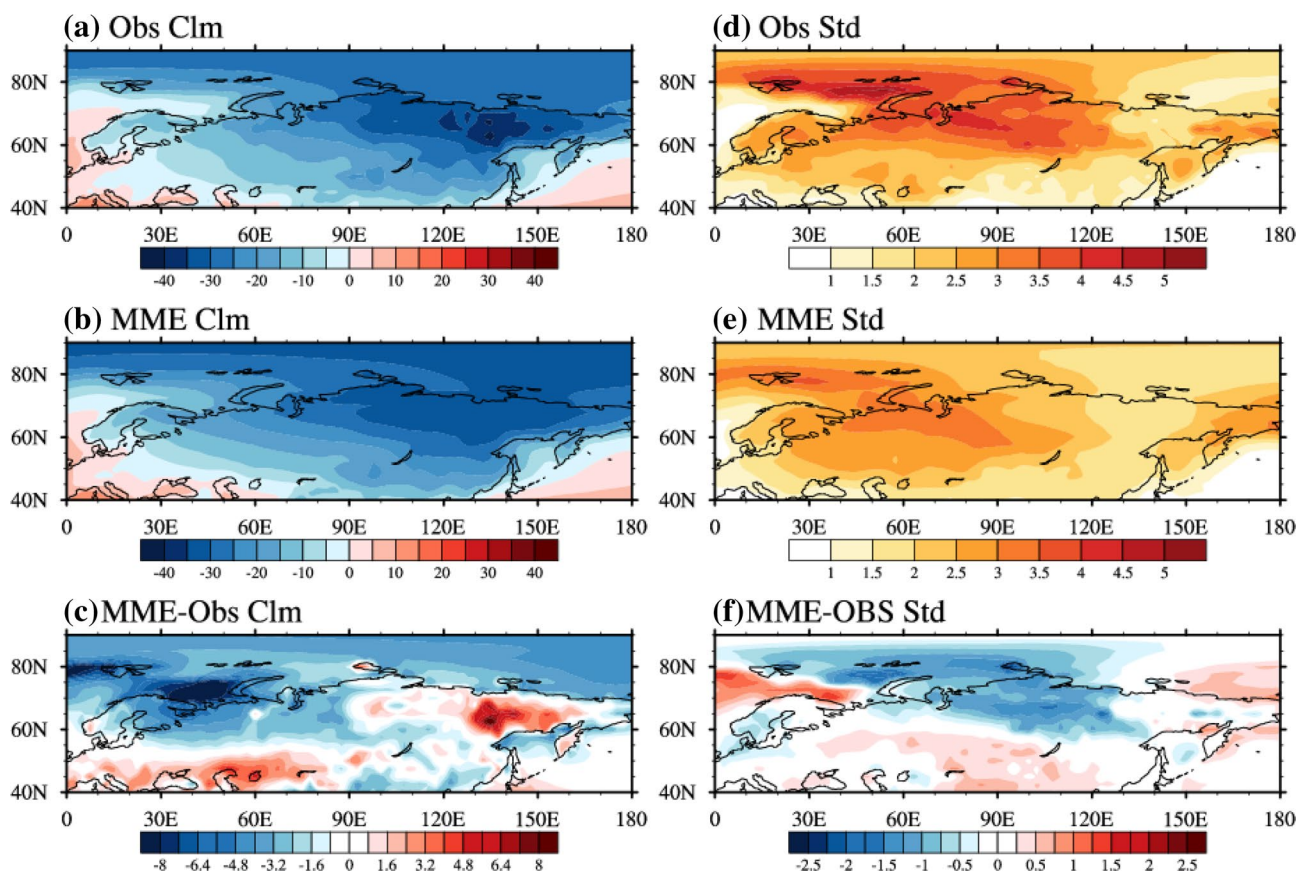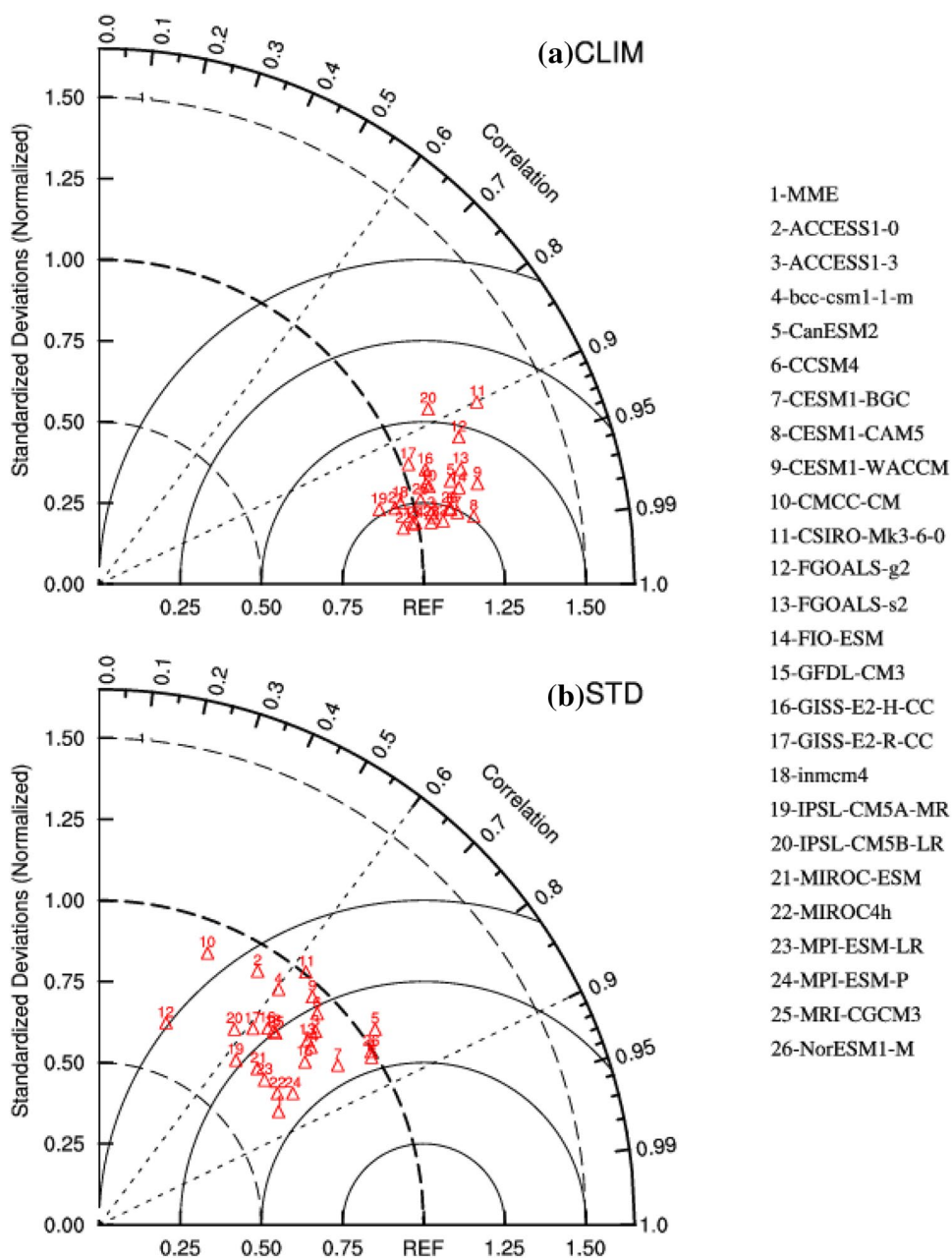
Fig. 1 **a** Observation (OBS), **b** ensemble mean of multiple models (MME) and **c** the difference between MME and OBS for the climatological SAT (shading; unit: °C) in winter. **d–f** Same as **a–c**, but for the standard deviation (shading; unit: °C)

about 6 °C in MME. Over Arctic, the climatological winter SAT is underestimated by about 8 °C in MME (Fig. 1c). For the STD in winter SAT variations, MME captures the large interannual variability over the Barents–Kara Seas region and northern Siberia, which is similar to the observed spatial feature (Fig. 1d). A difference map (Fig. 1f) indicates that the variance of winter SAT over most parts of the Arctic is underestimated in the MME. In contrast, MME tend to overestimate the variance of winter SAT over Eurasia.

To delineate the performance of the 25 models in representing the winter SAT in more detail, Taylor diagrams (Fig. 2) are plotted for the climatological and standard deviation of winter SAT within 40°–90° N, 0°–180° E. The climatological mean SAT in the individual models have high pattern correlation with the OBS and the corresponding correlation coefficients are above 0.90 in most of the models except for IPSL-CM5B-LR (Fig. 2a). This indicates that all of the 24 CMIP5 models can satisfactorily reproduce the spatial feature of climatological winter mean SAT. The normalized standard deviation ranges from 0.89 to 1.29. The spatial standard deviations are overestimated in most of the CMIP5 models, except for GFDL-CM3, inmcm4,

IPSL-CM5A-MR, MIROC-ESM, MIROC4h and MPI-ESM-P (Fig. 2a). The spatial distribution of climatological winter SAT in MME is better than that reproduced by most of the individual models, with a pattern correlation coefficient of 0.98 and a normalized standard deviation of 1.05 (Fig. 2a). For the STD, there exist large inter-model spreads in the pattern correlation coefficients and normalized standard deviation among the 25 CMIP5 models (Fig. 2b). The pattern correlations of winter mean SAT standard deviation ranges from 0.31 to 0.85, which are lower than those of the climatology (Fig. 2a, b). The pattern correlation coefficients are less than 0.6 in ACCESS1-0, CMCC-CM, FGOALS-g2 and IPSL-CM5B-LR (Fig. 2b). The CESM1-CAM5 and NorESM1-M are the two best models in capturing the standard deviation of the winter mean SAT over Eurasia in terms of pattern correlation coefficients (all larger than 0.84) (Fig. 2b). Furthermore, the normalized standard deviation ranges from 0.65 to 1.0. Similar to the climatology, the MME tends to have a higher capability than most of the individual models in reproducing the variance of the winter mean SAT with a pattern correlation coefficient of 0.85 and a normalized standard deviation of 0.65.

Fig. 2 Taylor diagram of **a** climatology and **b** standard deviation of winter SAT over the region of 40°–90° N and 0°–180° E. The pattern correlation between the CMIP5 models and observation is represented by the azimuthal position. The radial distance denotes the ratio of the standard deviation obtained from CMIP5 models to the standard deviation derived from observation

1-MME
2-ACCESS1-0
3-ACCESS1-3
4-bcc-csm1-1-m
5-CanESM2
6-CCSM4
7-CESM1-BGC
8-CESM1-CAM5
9-CESM1-WACCM
10-CMCC-CM
11-CSIRO-Mk3-6-0
12-FGOALS-g2
13-FGOALS-s2
14-FIO-ESM
15-GFDL-CM3
16-GISS-E2-H-CC
17-GISS-E2-R-CC
18-inmcm4
19-IPSL-CM5A-MR
20-IPSL-CM5B-LR
21-MIROC-ESM
22-MIROC4h
23-MPI-ESM-LR
24-MPI-ESM-P
25-MRI-CGCM3
26-NorESM1-M

4 WACE pattern and associated atmospheric circulation anomaly

Figure 3 is the regressed map of SAT, 300-hPa geopotential height (Z300), seal level pressure (SLP), 850-hPa wind on the normalized second principal components (PC2) both for MME and OBS. Figure 4 displays the explained variance of the EOF2 of winter SAT variations in the OBS and CMIP5 historical simulations during 1979–2005. In the OBS, the EOF2, which can explain 18.5% of the variance, exhibits a meridional dipole structure with centers over Arctic and Siberia (Fig. 3a). Consistent with Mori et al. (2014), the WACE pattern is closely related to the
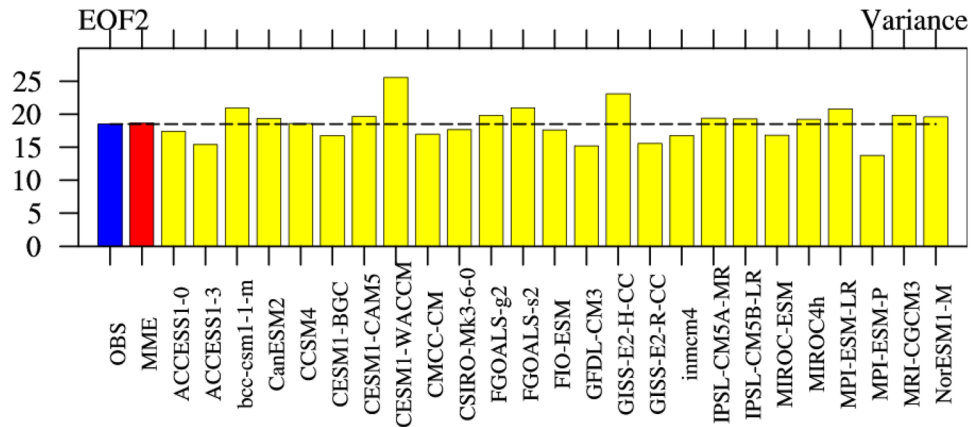
changes in the atmospheric circulation over Eurasia. As displayed in Fig. 3c, e, the positive phase of the WACE pattern is associated with positive geopotential height anomalies over Barents–Kara Sea region and negative geopotential height anomalies around Lake Baikal (Fig. 3c). This wave–train-like structure is quasi-barotropic and can extend to the surface (Fig. 3e). As demonstrated by Mori et al. (2014), the northerly cold-air advection accompanied by an anticyclonic circulation anomaly over northern Siberia causes cold SAT anomalies over the mid-latitude. The MME is generally able to reproduce the WACE pattern of SAT anomalies and associated atmospheric circulation anomalies, which is similar to the observed spatial feature
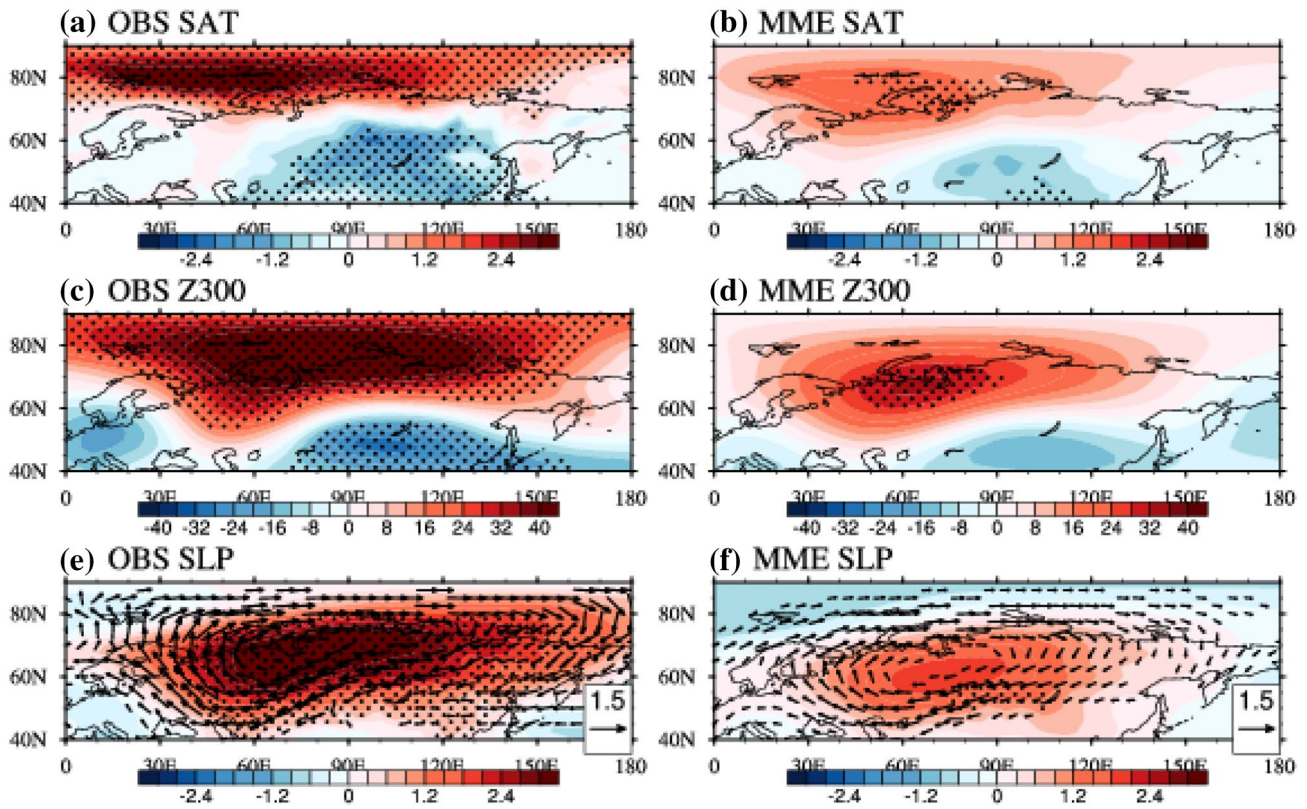
Fig. 3 Regressed winter SAT (shading; unit: °C) on normalized PC2 time series during 1979–2005 in the **a** OBS and **b** MME. **c**–**f** are the same as **a**, **b**, but for Z300 (shading; unit: m) and SLP (shading; unit:

hPa), respectively. Dots for shadings indicate the 90% confidence level. The vectors (units: ms^{-1}) in **e**, **f** denote the regressed 850 hPa wind on normalized PC2 time series

Fig. 4 Variance explained by the second EOF mode of winter SAT interannual variation over 40°–70° N and 0°–180° E in observations (blue bar) and CMIP5 historical simulations during 1979–2005. Red bar indicates MME of the 25 CMIP5 models, yellow bar indicates CMIP5 individual models


(Fig. 3b, d, f). However, the amplitude of the SAT anomalies and associated atmospheric circulation anomalies in MME is little weaker than that in OBS. The explained variance of the second EOF mode in MME is close to that in the observations (Fig. 4). The ACCESS1-0, ACCESS1-3, CESM1-BGC, CMCC-CM, CSIRO-Mk3-6-0, FIO-ESM, GFDL-CM3, GISS-E2-R-CC, inmcm4, MIROC-ESM and MPI-ESM-P reproduce smaller explained variances

(Fig. 4). In contrast, other 14 CMIP5 models overestimate the explained variances (Fig. 4).

To quantitatively estimate the performance of 25 CMIP5 models in representing the SAT anomalies associated with WACE pattern, the Taylor diagram is shown in Fig. 5. There exist large inter-model spreads in the pattern correlation coefficients and normalized standard deviation among the 25 CMIP5 models in simulating the WACE pattern (Fig. 5).

**Fig. 5** Same as Fig. 2, but for regressed winter SAT on normalized PC2 time series during 1979–2005
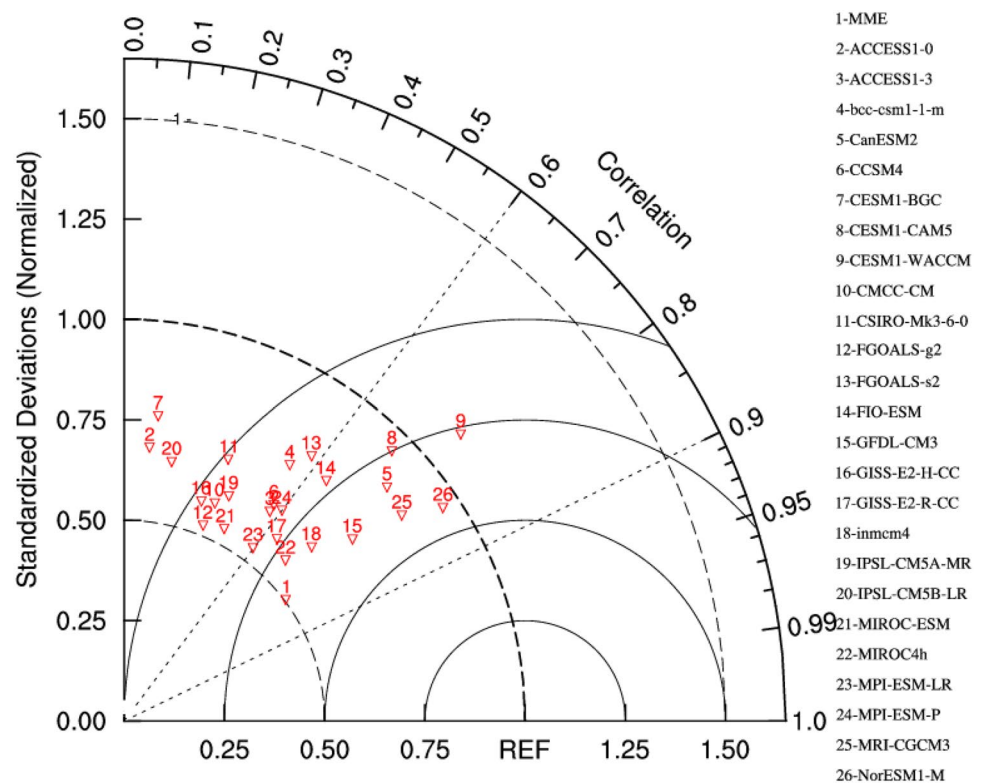
The pattern correlations of winter mean SAT anomalies over 0–180° E, 40°–90° N range from 0.09 to 0.83 (Fig. 5). The MRI-CGCM3 and NorESM1-M are the two best models in capturing the WACE pattern in terms of the pattern correlation coefficients (all larger than 0.8). The normalized standard deviation ranges from 0.5 to 1.1. Most of the CMIP5 models overestimate the spatial standard deviations except for CESM1-WACCM (Fig. 5). The MME is better than most of the individual models in representing the WACE pattern, with a pattern correlation coefficient of 0.8 and a normalized standard deviation of 0.5 (Fig. 5).

In the following, we further analyze the possible reasons responsible for the variations among the 25 CMIP5 models in reproducing the WACE pattern. High and low correlation model groups are selected in terms of the pattern correlation. According to the pattern correlation in Fig. 5, CanESM2, CESM1-WACCM, GFDL-CM3, MRI-CGCM3 and NorESM1-M are selected as the high correlation (HC) models (with pattern correlations larger than 0.75), and ACCESS1-0, CESM1-BGC, CMCC-CM, CSIRO-Mk3-6-0, FGOALS-g2, GISS-E2-H-CC and IPSL-CM5B-LR are defined as the low correlation (LC) models (with pattern correlations less than 0.39). Figure 6 compares MME anomalies of winter mean SAT, Z300, SLP and 850 hPa winds between HC and LC groups. Substantial differences in spatial characteristics and amplitude of the anomalous SAT are found between the HC and LC groups. In the MME of HC group, warm SAT anomalies appear over Barents–Kara

Seas region, and cold SAT anomalies occur over the Eurasian continent (Fig. 6a), and the results are consistent with the observations, despite little differences in the amplitude (Figs. 3a, 6a). Geopotential height anomalies at 300 hPa are featured by pronounced positive anomalies over the Arctic region and significant negative anomalies around Lake Baikal (Fig. 6c). In general, spatial patterns of the winter mean SAT and atmospheric circulation anomalies in the HC group bear a close resemblance to those in the observations (Figs. 3, 6a, c, e). In the MME of LC group, the dipole pattern is much weaker and shifts southeastward relative to that in the observations and HC group MME, so as the corresponding atmospheric circulation anomalies (Fig. 6b, d, f).

Chen et al. (2018) reported that the ability of a CMIP5 model in capturing the dominant mode of Eurasian spring SAT variations is connected with the model's performance while representing the related atmospheric circulation anomalies. From the Fig. 6, it is assumed that the ability of the CMIP5 models in reproducing the WACE pattern may be closely related to the performance of the models in capturing the observed atmospheric circulation pattern. Evidence is presented in the following section to verify the above assertion. Figure 7 displays a scatter diagram of the pattern correlation of SAT anomalies against the pattern correlation of Z300 anomalies and 850 hPa wind anomalies in the region bounded within 40°–90° N, 0°–180° E. Results in Fig. 7 suggest that the CMIP5 models which have larger pattern correlations for Z300 anomalies and 850 hPa wind
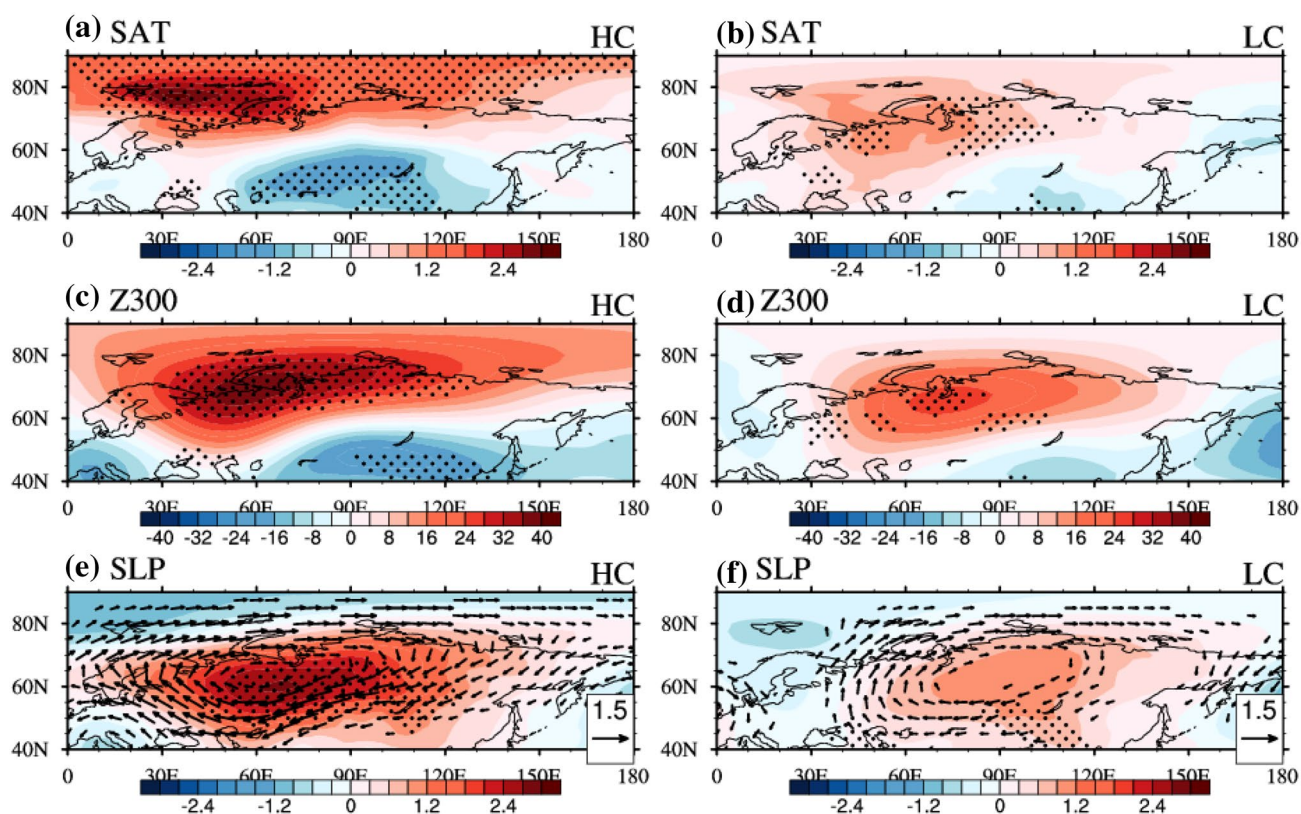
Fig. 6 MME anomalies of winter SAT (shading; unit: °C) obtained by regression upon normalized PC2 time series during 1979–2005 in the **a** HC and **b** LC groups. **c–f** Same as **a**, **b**, but for Z300 (shading; unit: m) and SLP (shading; unit: hPa), respectively. Dots for shadings indicate the 90% confidence level. The vectors (units: ms^{-1}) in **e**, **f** denote the regressed 850 hPa wind anomalies

anomalies tend to have larger pattern correlation for SAT anomalies over the region within 40°–90° N, 0°–180° E. The correlation coefficients between the two variables presented in Fig. 7a, b are as high as 0.74 and 0.78, respectively, which are significant at the 99% confidence level according to the Student's t test. The evidence confirms the assertion that CMIP5 model's performance in representing the SAT anomalies related to the WACE pattern is closely associated with the model's ability in capturing the atmospheric circulation pattern over Eurasia.

Considering previous studies have reported that the "Warm Arctic, Cold Continents" pattern in winter SAT is induced by sea ice loss (Honda et al. 2009; Liu et al. 2012; Mori et al. 2014; Kug et al. 2015), we further examine the interannual relationship between sea ice loss and WACE pattern. Figure 8 display the anomalies of SIC in autumn and winter, which are regressed on the normalized PC2 time series for the periods of 1979–2005 in OBS. In autumn, significant negative SIC anomalies were observed in the northern Barents Sea and the Kara Sea (Fig. 8a). In winter, the SIC anomalies over Barents–Kara Seas shifted southward relative to those in autumn (Fig. 8b). These results indicate a significant connection between the WACE pattern and

autumn and winter SIC anomalies around the Barents–Kara Sea. Hence, it is worthy to investigate whether CMIP5 models' biases in reproducing the WACE pattern were related to the model's ability in capturing the relationship between the SIC anomalies and the WACE pattern? Fig. 9 displays the MME anomalies of autumn and winter SIC, which is obtained by regressing on the normalized PC2 time series in the HC and LC groups, respectively. However, unlike the observational findings obtained in Fig. 9a, the SIC anomalies in autumn are weaker and insignificant in the Barents–Kara seas region both for the HC and LC model groups (Fig. 9a, c). In winter, significant decrease in SIC can be observed over Barents–Kara Seas in HC model groups, while no winter SIC signal can be seen for LC model group during the positive phase of the WACE pattern (Fig. 9b,d).

Therefore, the ability of the CMIP5 model in simulating the WACE pattern may be partly related to the model's performance in capturing its connection with the winter SIC over the Barents–Kara Seas. To confirm this assertion, we calculate the correlation coefficient between the winter mean SIC index and the PC2 time series in the HC and LC model group and the results are shown in Fig. 10. The SIC index is defined as domain average SIC over Barents–Kara
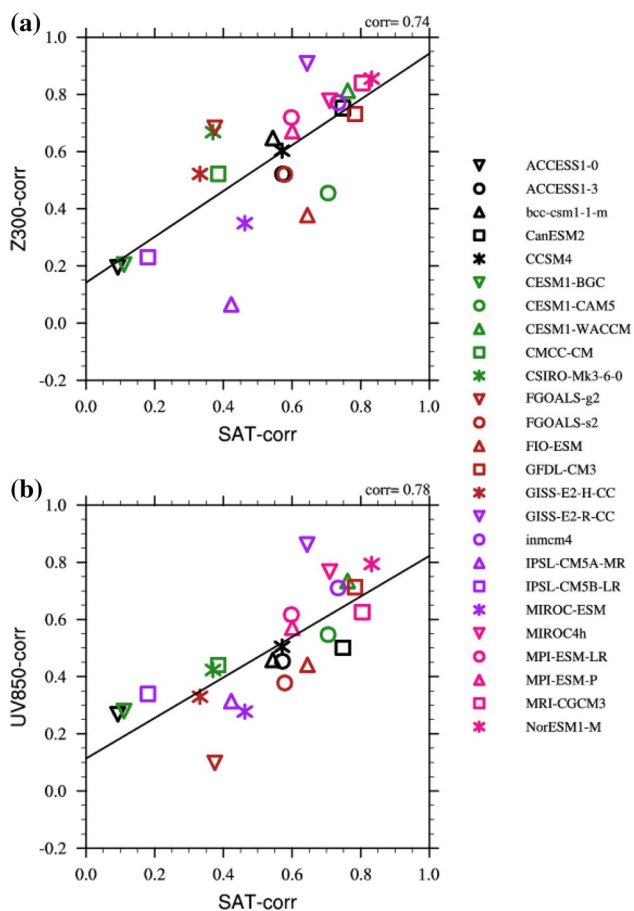
Fig. 7 Scatterplot of pattern correlation between the observed and simulated SAT anomalies vs **a** pattern correlation between the observed and simulated Z300 anomalies, and **b** pattern correlation between the observed and simulated 850 hPa wind anomalies over 40°–90° N and 0°–180° E. The best fitting line is represented by the black solid line in **a** and **b**

Seas (10°–60° E, 70°–80° N). The SIC index has been multiplied by − 1 for the simplicity of comparison. In LC model group, except for the IPSL-CM5B-LR, the correlation coefficients in ACCES1-0, CESM1-BGC, CMCC-CM, CSIRO-Mk3-6-0, FGOALS-s2, GISS-E2-R-CC are all below the 95% confidence level. In the HC model group (i.e., CanESM2, CESM1-WACCM, MRI-CGCM3, NorESM1-M), the correlation coefficients between the SIC index and the PC2 time series all exceeds the 99% confidence level. This indicates that the ability of CMIP5 model in simulating the WACE pattern may be due to the model's ability in capturing the relationship between the WACE pattern and the winter SIC over the Barents–Kara Seas.

Mori et al. (2014) has reported that WACE pattern is closely related to the winter SIC over Barents–Kara Seas. In particular, they reported that SIC-driven atmospheric response favors cold-air advection to Eurasia. This implies that the ability of the CMIP5 model in capturing the WACE pattern is closely related to the model's performance in simulating the atmospheric circulation anomalies associated with the SIC over Barents–Kara Seas. To address this issue, we have compared the spatial patterns of winter mean SAT and Z300 anomalies corresponding to the sea ice loss over Barents–Kara Seas between the HC and LC model groups. Figure 11 displays MME anomalies of winter mean SAT and Z300 anomalies, which are obtained by regression upon the normalized SIC index in the HC and LC groups, respectively. In the MME of the HC group, spatial distributions pattern of SAT and Z300 anomalies resembles those shown in Fig. 3a, c. Sea ice loss in the Barents–Kara Seas correspond well to the warm anomalies over Barents–Kara Seas and cold anomalies over Siberia (Fig. 11a). Geopotential height anomalies at 300 hPa exhibit positive anomalies over Arctic region and negative anomalies around Lake Baikal region (Fig. 11c). Therefore, sea ice loss in the Barents–Kara Seas appears to initiate eastward-propagating wave trains of alternative high- and low-pressure regions in the HC group.

Fig. 8 Anomalies of **a** autumn and **b** winter SIC (shading; unit:%) regressed upon the normalized PC2 time series during 1979–2005 in OBS. Dots for shadings indicate the 90% confidence level
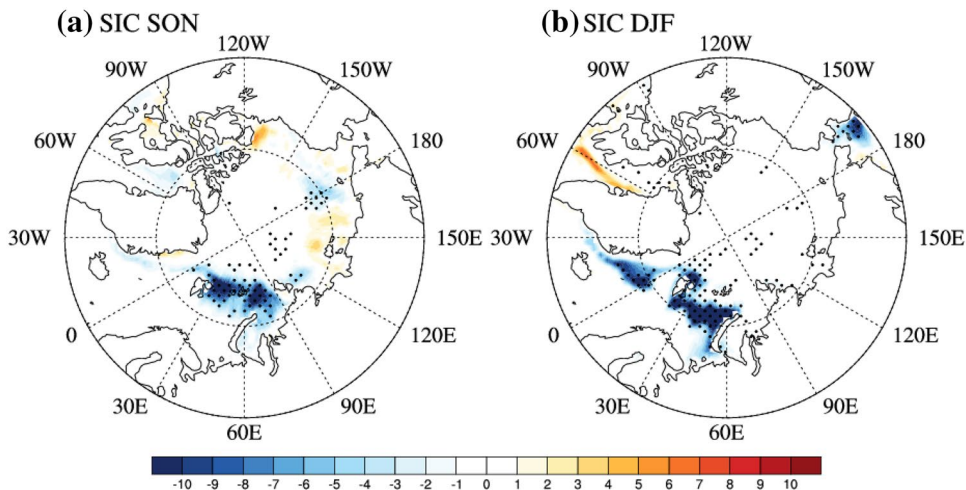
Fig. 9 MME anomalies of autumn SIC (shading; unit: %) obtained by regression upon the normalized PC2 time series during 1979–2005 in the **a** HC and **b** LC groups, respectively. **c**, **d** same as **a**, **b**, but for winter SIC (shading; unit: %). Dots for shadings indicate the 90% confidence level
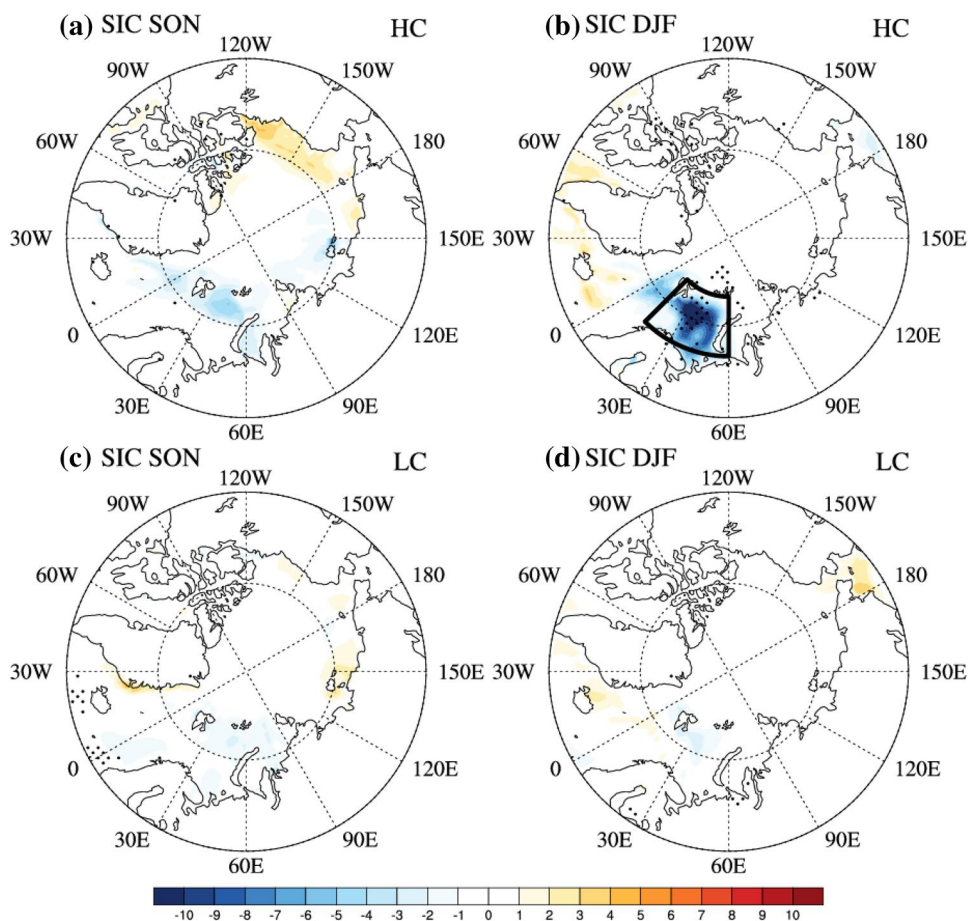
Fig. 10 Correlation coefficients between the winter SIC index and normalized PC2 time series during 1979–2005 in the (red bars) HC and (yellow bars) LC model groups. The horizontal dashed lines indicate the correlation coefficient significant at the 95% and 99% confidence level, respectively
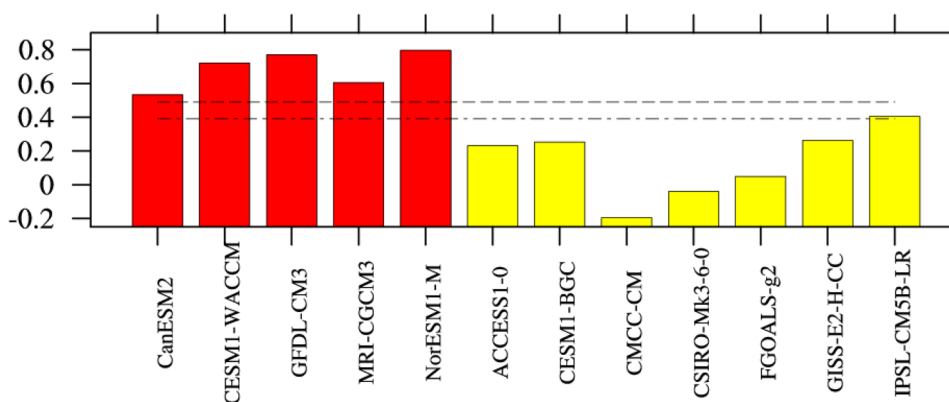
Anomalous high pressures around the Barents–Kara Seas triggers advection of anomalous cold air deep inside central and East Asia. Contrastingly, in the LC group, the sea ice driven Rossby wave and associated SAT anomalies are weaker and insignificant (Fig. 11b, d). The above analysis suggests a higher ability of the CMIP5 models in HC group in reproducing the atmospheric variations induced by sea ice loss.

Furthermore, we investigate the possible origin of the CMIP5 models' biases in capturing the winter SIC-related

atmospheric circulation anomalies. The differences in standard deviations of winter mean SIC between the HC group and the LC group is displayed in Fig. 12a. Since the linkage between SIC over the Barents–Kara Seas and wintertime surface climate anomalies over Eurasia may depend on the strength of the standard deviations of winter mean SIC (Fan et al. 2017). As shown in Fig. 12a, the standard deviations of SIC in the northern Barents Sea and the Kara Sea in the HC group are larger than those in the LC group. Therefore, the stronger influences of winter mean SIC on
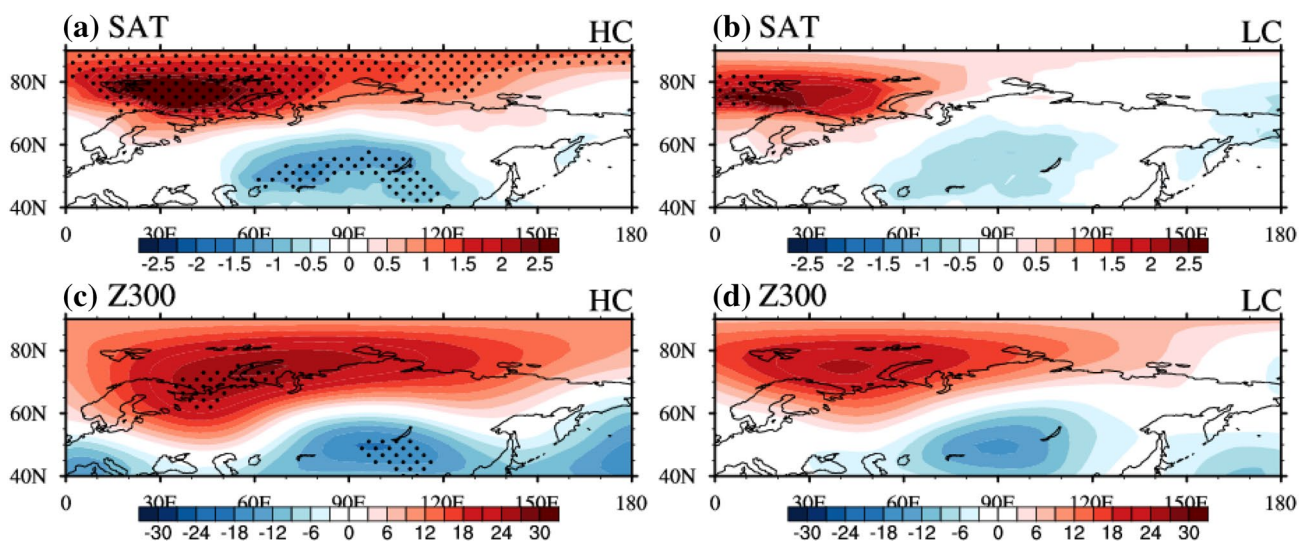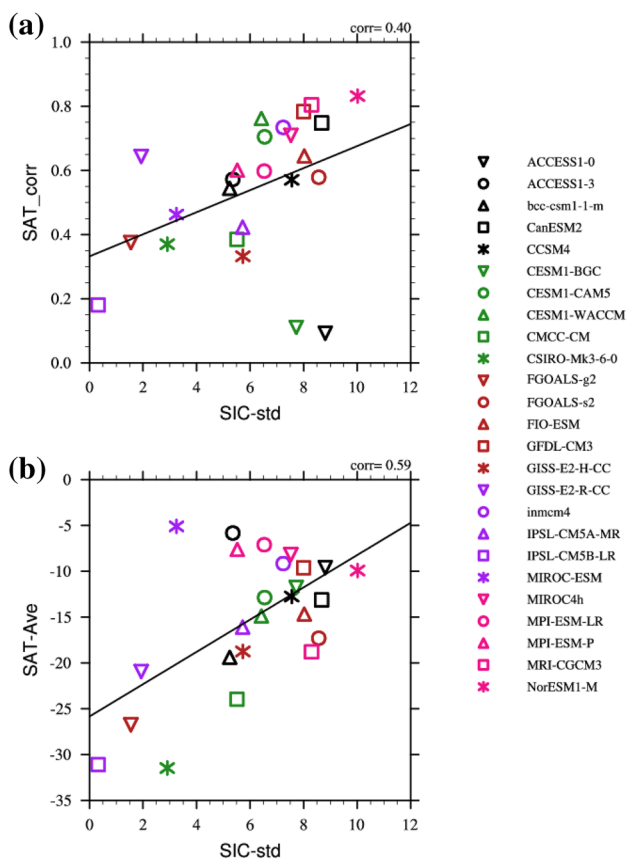
Fig. 11 MME anomalies of winter SAT (shading; unit: °C) obtained by regression upon the normalized SIC index during 1979–2005 in the **a** HC and **b** LC groups, respectively. **c**, **d** are the same as **a**, **b**, but for Z300 (shading; unit: m). Dots for shadings indicate the 90% confidence level

Fig. 12 The difference of **a** standard deviation of winter SIC (shading; unit: %) and **b** climatological winter SAT during 1979–2005 between HC and LC groups
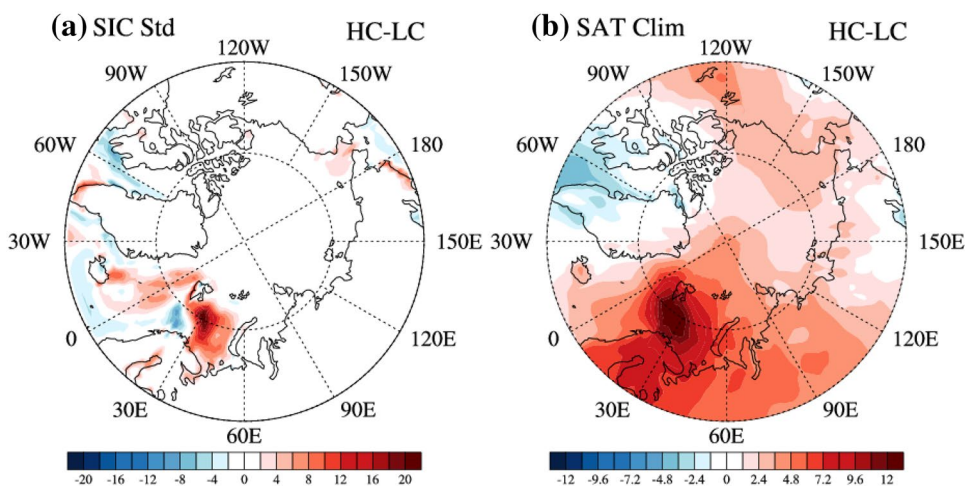
the atmospheric circulation anomalies in the HC group may be due to the larger standard deviations of winter SIC simulated in HC group. As warmer Arctic can lead to less and thinner sea ice, which tend to have larger year-to-year variability, it is assumed that the larger year-to-year variability of SIC over the Barents–Kara Seas in the HC group might be due to higher SAT. Figure 12b display the differences in winter mean SAT averaged from 1979 to 2005 between the HC group and LC group. It shows that warmer SAT can be observed over northern Barents Sea and the Kara Sea in the HC group, implying that higher SAT can lead to larger standard deviations in SIC. According to the above analysis, it is assumed that the ability of the CMIP5 models in reproducing the WACE pattern is closely related to the inter-model diversity in the strength of the standard deviations of winter SIC over the Barents–Kara Seas. The above assertion
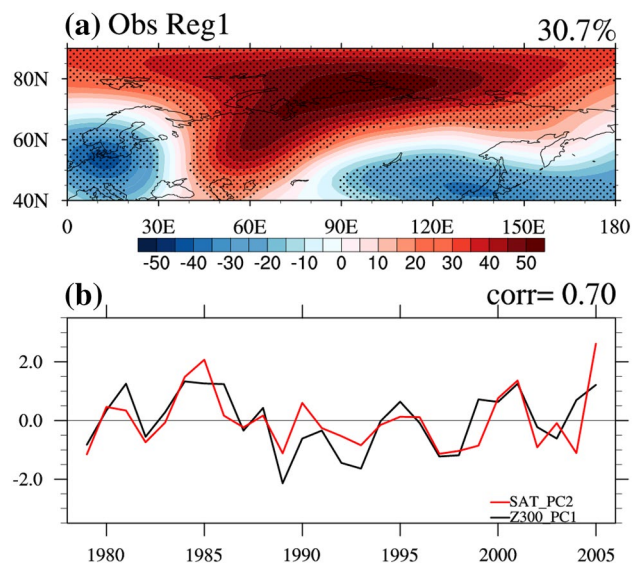
is verified by the relationship between the pattern correlation of pattern correlation of SAT anomalies and STD of SIC over the Barents–Kara Seas. Figure 13a shows a scatter diagram in which the x and y axes represent the STD of SIC and the pattern correlation of SAT anomalies, respectively, based on 25 CMIP5 model simulations. The figure reveals that larger SIC variability (i.e., larger STD) corresponds a high pattern correlation of SAT anomalies in most of the CMIP5 models. The correlation coefficient between x and y variables is 0.40 (Fig. 13a), exceeding the 95% confidence level. Furthermore, the inter-model diversity in the simulated SIC variability might be caused by the inter-model diversity in the mean state of winter SAT. Similarly, Fig. 13b shows a scatter diagram of the STD of SIC against the domain average winter mean SAT over the Barents–Kara Sea averaged from 1979 to 2004. Results in Fig. 13b suggest that the

(a)

(b)

(a) Obs Reg1

30.7%

(b)

corr= 0.70

Fig. 14 a Anomalies of winter Z300 (shading; m) obtained by regressed upon the normalized PC time series of the EOF1 of winter Z300 over 40°–90° N and 0°–180° E during 1979–2005 and **b** the corresponding normalized PC time series. The normalized PC time series of the EOF2 of the winter mean SAT over 40°–90° N and 0°–180° E was also displayed in **b** for comparison. Dots for shadings indicate the 90% confidence level

Fig. 13 Scatterplot of standard deviation of SIC index vs **a** pattern correlation between the observed and simulated SAT, and **b** domain average SAT over Barents–Kara Seas (70°–80° N, 10°–60° E) average from 1979 to 2005. The best fitting line is represented by the black solid line in **a** and **b**

CMIP5 models that have higher SAT over the Barents–Kara Seas tend to produce larger SIC STD. The correlation coefficient between the two variables, presented in Fig. 13b is 0.59, which is significant at 99% confidence level according to the Student's t test. These evidences confirm the assertion that CMIP5 model's performance in representing the SAT anomalies related to the WACE pattern is partly due to amplitude of SIC variability among the CMIP5 models. Additionally, it is indicated that the inter-model diversity in the simulated SIC variability is partly caused by the inter-model diversity in the mean state of winter SAT.

Chen et al. (2018) reported that the ability of the CMIP5 model in capturing the dominant mode of the spring Eurasian SAT is closely related to the model's performance in simulating the dominant mode of the spring atmospheric circulation variations over Eurasia. Therefore, the question is whether CMIP5 models' biases in reproducing the WACE pattern are related to the model's ability in model's performance while simulating the dominant mode of the winter atmospheric circulation variabilities over Eurasia.

Figure 14a displays the EOF1 of winter Z300 anomalies over 40°–90° N, 0°–140° E in OBS. It is found that the spatial distributions of the EOF1 of winter Z300 anomalies bear several resemblances to those shown in Fig. 3c. Furthermore, there is a significant connection between the WACE pattern and the EOF1 of winter Z300 anomalies. The correlation coefficient between the PC time series is around 0.70 (Fig. 14b).

The linkage between the dominant mode of the winter atmospheric circulation patterns and WACE pattern has been confirmed in the observations. To check whether CMIP5 models' biases in reproducing the WACE pattern are related to the model's ability in simulating the dominant mode of the winter atmospheric circulation variations over Eurasia, we compared the spatial patterns corresponding to the EOF1 of winter mean Z300 anomalies between the HC and LC model groups. Figure 15 displays MME anomalies of winter mean Z300 anomalies obtained by regressing the normalized PC time series of EOF1 on winter mean Z300 anomalies in the HC and LC groups, respectively. However, there are no pronounced differences in the spatial patterns of the atmospheric circulation anomalies related to EOF1 of the winter mean Z300 variations. The spatial distributions of the atmospheric circulation anomalies both in HC and LC groups bear several resemblances to those shown in Fig. 3c. Above analysis suggests a weaker connection between the ability of a CMIP5 model in capturing the WACE pattern and the
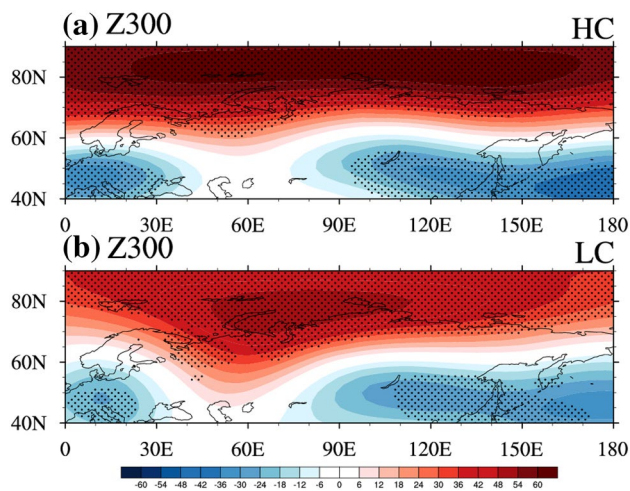
Fig. 15 MME anomalies of winter Z300 (shading; m) obtained by regression upon the normalized PC time series of the EOF1 of winter Z300 over 40°–90° N and 0°–180° E during 1979–2005 in the **a** HC and **b** LC groups, respectively. Dots for shadings indicate the 90% confidence level

model's performance in reproducing the dominant mode of the winter Eurasian atmospheric variations.

5 Summary

The present study defined the EOF2 of winter mean SAT over 0°–180° E, 40°–90° N during 1979–2005 as WACE pattern. This study analyzes the performance of 25 CMIP5 models in capturing the WACE pattern based on the historical simulations, as well as the climatology and standard deviation of winter mean SAT in the study region. The MME satisfactorily reproduces the observed spatial structure of climatological winter SAT over the region spanning from northern Eurasia to Arctic. The MME underestimates the SAT climatology over Barents Seas by about 8 °C and overestimates the climatology around the Caspian Sea by about 6 °C. Most of the 25 CMIP5 models satisfactorily reproduce the spatial feature of climatological winter mean SAT, with the pattern correlation coefficients larger than 0.90, except for IPSL-CM5B-LR. In the MME, the standard deviations of winter mean SAT over the Barents–Kara Seas were underestimated. Large spread in the simulation of the standard deviation of the winter mean SAT can be found among the 25 CMIP5 models. The pattern correlations of winter mean SAT standard deviation ranges from 0.31 to 0.85 in the individual models, which are much lower than those of the winter climatology. The spatial pattern of the anomalies of SAT, Z300 and SLP associated with the WACE pattern in MME is close to that in the observations, but with smaller amplitude. The simulation of the WACE pattern in

each model exhibits large spread in terms of pattern correlation coefficient. Then 5 HC (CanESM2, CESM1-WACCM, GFDL-CM3, MRI-CGCM3 and NorESM1-M) and 7 LC (ACCESS1-0, CESM1-BGC, CMCC-CM, CSIRO-Mk3-6-0, FGOALS-g2, GISS-E2-H-CC and IPSL-CM5B-LR) models are selected according to the pattern correlation. The HC models exhibit a better simulation ability of the WACE pattern and associated atmospheric circulation anomalies compared to the LC models. Furthermore, the winter mean SIC over the Barents–Kara Seas exhibit closer link to the WACE pattern and associated atmospheric circulation anomalies in HC group than that in the LC group. It further indicates that the ability of the CMIP5 models in reproducing the WACE pattern is closely related to the model's performance in representing the observed atmospheric circulation anomalies related to the winter mean SIC variation over the Barents–Kara Seas, which is partly due to the strength of the simulated SIC variability. Larger standard deviations of winter SIC over Barents–Kara Seas can easily induce stronger and southward propagating stationary Rossby wave train, which further induce the winter mean SAT anomalies associated with the WACE pattern.

6 Discussion

Many studies have demonstrated that autumn Arctic sea ice plays a critical role in the winter mean atmospheric circulation (Francis et al. 2009; Overland and Wang 2010; Hopsch et al. 2012; Jaiser et al. 2012; Chen et al. 2014) and mid-latitude Eurasian cold winters (Liu et al. 2012). Our observational analysis also reveals that WACE pattern is closely related to sea ice loss in autumn (Fig. 8a). However, different from the observational findings, the SIC anomalies in the autumn exhibits weak and insignificant connection with the WACE pattern of winter mean SAT both for the HC and LC model groups (Fig. 9a, c). According to Chen et al. (2014), on the interanuanl time scale, autumn Arctic SIC anomalies affect the winter mean Asian circulation through atmospheric processes (Alexander et al. 2003; Deser et al. 2004, 2007; Honda et al. 2009; Chen et al. 2014). Specifically, anomalous autumn SIC-induced thermal state leads to an atmospheric circulation change around the Arctic and then the circulation change extends to Asia in winter through atmospheric processes such as the wave activity fluxes (Alexander et al. 2003; Deser et al. 2004, 2007; Honda et al. 2009; Chen et al. 2014). The failure of CMIP5 models in capturing the link between autumn SIC anomalies and winter Asian circulation may be due to their poor performances in reproducing the atmospheric processes, such as transient eddy feedback. Furthermore, previous studies with model simulations have reported that autumn sea ice loss over the Barents–Kara Seas can trigger cold weather over Eurasia

through stratospheric pathway (Kim et al. 2014; Zhang et al. 2018), indicating the importance of stratosphere-troposphere coupling process. They reported that low-top models or models with an insufficiently resolved stratosphere exhibit weaker stratosphere-troposphere coupling than that in observations or high-top stratosphere-resolving models (Charlton-Perez et al. 2013; Osprey et al. 2013). However, most of the CMIP5 models are 'low-top' models only, which poorly resolves the stratosphere and stratosphere–troposphere coupling mechanisms (Charlton-Perez et al. 2013). It may be another factor responsible for the unsuccessful representation of the linkage between the WACE and autumn sea ice loss over Barents–Kara Seas.

Our study emphasized that the ability of the CMIP5 model in representing the observed atmospheric circulation anomalies related to the winter SIC variation over Barents–Kara Seas is partly due to their performance in simulating the SIC variability. The inter-model diversity of the simulated SIC variability may be caused by the inter-model spread in simulation of the sea ice thickness, which needs to be verified in the future. It should be noted that the atmospheric circulation response to the sea ice changes is also sensitive to the background climatic state (Kushnir et al. 2002; Balmaseda et al. 2010; Overland et al. 2016; Screen and Francis 2016; Sung et al. 2016; Li et al. 2018). For example, Li et al. (2018) suggested that the linkage between the sea ice cover in the Atlantic sector of Arctic and Eurasian climate only manifests in the cold phase of the Atlantic Multidecadal Oscillation (Li et al. 2018). Therefore, whether the performance of CMIP5 models in simulating the background climatic state can affect their ability to represent the WACE pattern needs to be studied in the future.

Compliance with ethical standards

References

Alexander MA, Bhatt US, Walsh JE, Timlin MS, Miller JS, Scott JD (2003) The atmospheric response to realistic Arctic sea ice anomalies in an AGCM during winter. J Clim 17:890–905

Balmaseda MA, Ferranti L, Molteni F, Palmer TN (2010) Impact of 2007 and 2008 Arctic ice anomalies on the atmospheric circulation: implications for long-range predictions. Q J R Meteorol Soc 136:1655–1664

Charlton-Perez AJ et al (2013) On the lack of stratospheric dynamical variability in low-top versions of the CMIP5 models. J Geophys Res Atmos 118:2494–2505

Chen Z, Wu R, Chen W (2014) Impacts of Autumn Arctic sea ice concentration changes on the East Asian Winter Monsoon variability. J Clim 27:5433–5450. https://doi.org/10.1175/jcli-d-13-00731.1

Chen S, Wu R, Song L, Chen W (2018) Present-day status and future projection of spring Eurasian surface air temperature in CMIP5 model simulations. Clim Dyn 52:5431–5449

Cohen JL, Furtado JC, Barlow M, Alexeev VA, Cherry JE (2012a) Asymmetric seasonal temperature trends. Geophys Res Lett 39:54–62

Cohen JL, Furtado JC, Barlow MA, Alexeev VA, Cherry JE (2012b) Arctic warming, increasing snow cover and widespread boreal winter cooling. Environ Res Lett 7:014007. https://doi.org/10.1088/1748-9326/7/1/014007

Cohen J, Jones J, Furtado J, Tziperman E (2013) Warm Arctic, cold continents: a common pattern related to Arctic sea ice melt, snow advance, and extreme winter weather. Oceanography. https://doi.org/10.5670/oceanog.2013.70

Cohen J et al (2014) Recent Arctic amplification and extreme mid-latitude weather. Nat Geosci 7:627–637. https://doi.org/10.1038/ngeo2234

Cohen J et al (2020) Divergent consensuses on Arctic amplification influence on midlatitude severe winter weather. Nat Clim Change 10:20–29. https://doi.org/10.1038/s41558-019-0662-y

Dee DP et al (2011) The ERA-Interim reanalysis: configuration and performance of the data assimilation system. Q J R Meteorol Soc 137:553–597. https://doi.org/10.1002/qj.828

Deser C, Magnusdottir G, Saravanan R, Phillips A (2004) The effects of North Atlantic SST and sea ice anomalies on the winter circulation in CCM3. Part II: direct and indirect components of the response. J Clim 17:877–889

Deser C, Tomas RA, Peng S (2007) The transient atmospheric circulation response to North Atlantic SST and sea ice anomalies. J Clim 20:4751

Fan K, Xie Z, Wang H, Xu Z, Liu J (2017) Frequency of spring dust weather in North China linked to sea ice variability in the Barents Sea. Clim Dyn. https://doi.org/10.1007/s00382-016-3515-7

Francis JA, Vavrus SJ (2012) Evidence linking Arctic amplification to extreme weather in mid-latitudes. Geophys Res Lett 39:L06801. https://doi.org/10.1029/2012gl051000

Francis JA, Chan W, Leathers DJ, Miller JR, Veron DE (2009) Winter Northern Hemisphere weather patterns remember summer Arctic sea-ice extent. Geophys Res Lett 36:157–163

Guo Y, Zhao Z, Dong W (2016) Two dominant modes of winter temperature variations over China and their relationships with large-scale circulations in CMIP5 models. Theor Appl Climatol 124:579–592

Honda M, Inoue J, Yamane S (2009) Influence of low Arctic sea-ice minima on anomalously cold Eurasian winters. Geophys Res Lett 36:L08707. https://doi.org/10.1029/2008gl037079

Hopsch S, Cohen J, Dethloff K (2012) Analysis of a link between fall Arctic sea ice concentration and atmospheric patterns in the following winter. Tellus A 64:18624. https://doi.org/10.3402/tellusa.v64i0.18624

Inoue J, Hori ME, Takaya K (2012) The role of Barents sea ice in the wintertime cyclone track and emergence of a Warm-Arctic Cold-Siberian anomaly. J Clim 25:2561–2568. https://doi.org/10.1175/jcli-d-11-00449.1

Jaiser R, Dethloff K, Handorf D, Rinke A, Cohen J (2012) Impact of sea ice cover changes on the Northern Hemisphere atmospheric

winter circulation. Tellus A. https://doi.org/10.3402/tellusa.v64i0.11595

Jeong J-H, Ou T, Linderholm HW, Kim B-M, Kim S-J, Kug J-S, Chen D (2011) Recent recovery of the Siberian High intensity. J Geophys Res 116:D23102. https://doi.org/10.1029/2011jd015904

Johannessen OM et al (2004) Arctic climate change: observed and modeled temperature and sea-ice variability. Tellus A 56:559–560. https://doi.org/10.1111/j.1600-0870.2004.00092.x

Kim BM et al (2014) Weakening of the stratospheric polar vortex by Arctic sea-ice loss. Nat Commun 5:4646. https://doi.org/10.1038/ncomms5646

Kug JS, Jeong JH, Jang YS, Kim BM, Folland CK, Min SK, Son SW (2015) Two distinct influences of Arctic warming on cold winters over North America and East Asia. Nat Geosci 8:759–762. https://doi.org/10.1038/ngeo2517

Kushnir Y, Robinson WA, Bladé I, Hall NMJ, Peng S, Sutton R (2002) Atmospheric GCM response to extratropical SST anomalies: synthesis and evaluation. J Clim 15:2233–2256

Li F, Orsolini YJ, Wang H, Gao Y, He S (2018) Atlantic Multidecadal Oscillation modulates the impacts of Arctic sea ice decline. Geophys Res Lett 45:2497–2506

Liang YC et al (2019) Quantification of the Arctic Sea Ice-Driven Atmospheric Circulation Variability in Coordinated Large Ensemble Simulations. Geophys Res Lett 47:1. https://doi.org/10.1029/2019GL085397

Lindsay R, Wensnahan M, Schweiger A, Zhang J (2014) Evaluation of seven different atmospheric reanalysis products in the Arctic. J Clim 27:2588–2606

Liu J, Curry JA, Wang H, Song M, Horton RM (2012) Impact of declining Arctic sea ice on winter snowfall. Proc Natl Acad Sci USA 109:4074

Miao C et al (2014) Assessment of CMIP5 climate models and projected temperature changes over Northern Eurasia. Environ Res Lett 9:055007

Mori M, Watanabe M, Shiogama H, Inoue J, Kimoto M (2014) Robust Arctic sea-ice influence on the frequent Eurasian cold winters in past decades. Nat Geosci 7:869–873. https://doi.org/10.1038/ngeo2277

North GR, Moeng FJ, Bell TL, Cahalan RF (1982) The latitude dependenceof the variance of zonally averaged quantities. Mon Weather Rev 110:319–326. https://doi.org/10.1175/1520-0493(1982)110%3c0319:Tldotv%3e2.0.Co;2

Osprey SM, Gray LJ, Hardiman SC, Butchart N, Hinton TJ (2013) Stratospheric variability in twentieth-century CMIP5 simulations of the Met Office climate model: high top versus low top. J Clim 26:1595–1606

Overland JE, Wang M (2010) Large-scale atmospheric circulation changes are associated with the recent loss of Arctic sea ice. Tellus A 62:1–9. https://doi.org/10.1111/j.1600-0870.2009.00421.x

Overland JE, Wood KR, Wang M (2010) Warm Arctic—cold continents: climate impacts of the newly open Arctic Sea. Polar Res 30:157–171

Overland JE et al (2016) Nonlinear response of mid-latitude weather to the changing Arctic. Nat Clim Change 6:992–999. https://doi.org/10.1038/nclimate3121

Park DSR, Lee S, Feldstein SB (2015) Attribution of the recent winter sea ice decline over the Atlantic sector of the Arctic Ocean. J Clim 28:4027–4033

Peings Y, Magnusdottir G (2014) Response of the wintertime Northern Hemisphere atmospheric circulation to current and projected Arctic sea ice decline: a numerical study with CAM5. J Clim 27:244–264

Polyakov IV et al (2002) Observationally based assessment of polar amplification of global warming. Geophys Res Lett 29:1878. https://doi.org/10.1029/2001gl011111

Rayner NA et al (2003) Global analyses of sea surface temperature, sea ice, and night marine air temperature since the late nineteenth century. J Geophys Res 108:407. https://doi.org/10.1029/2002jd002670

Screen JA, Francis JA (2016) Contribution of sea-ice loss to Arctic amplification is regulated by Pacific Ocean decadal variability. Nat Clim Change 6:856–860. https://doi.org/10.1038/nclimate3011

Screen JA, Simmonds I (2010a) The central role of diminishing sea ice in recent Arctic temperature amplification. Nature 464:1334–1337. https://doi.org/10.1038/nature09051

Screen JA, Simmonds I (2010b) Increasing fall-winter energy loss from the Arctic Ocean and its role in Arctic temperature amplification. Geophys Res Lett 37:L16707. https://doi.org/10.1029/2010gl044136

Screen JA, Deser C, Simmonds I (2012) Local and remote controls on observed Arctic warming. Geophys Res Lett 39:L10709. https://doi.org/10.1029/2012gl051598

Screen JA, Simmonds I, Deser C, Tomas R (2013) The Atmospheric response to three decades of observed Arctic sea ice loss. J Clim 26:1230–1248. https://doi.org/10.1175/jcli-d-12-00063.1

Serreze MC, Barry RG (2011) Processes and impacts of Arctic amplification: a research synthesis. Glob Planet Change 77:85–96. https://doi.org/10.1016/j.gloplacha.2011.03.004

Sun L, Perlwitz J, Hoerling M (2016) What caused the recent "Warm Arctic, Cold Continents" trend pattern in winter temperatures? Geophys Res Lett 43:5345–5352. https://doi.org/10.1002/2016gl069024

Sung MK, Kim BM, Baek EH, Lim YK, Kim SJ (2016) Arctic-North Pacific coupled impacts on the late autumn cold in North America. Environ Res Lett 11:084016

Tang Q, Zhang X, Yang X, Francis JA (2013) Cold winter extremes in northern continents linked to Arctic sea ice loss. Environ Res Lett 8:014036. https://doi.org/10.1088/1748-9326/8/1/014036

Taylor KE (2001) Summarizing multiple aspects of model performance in a single diagram. J Geophys Res 106:7183–7192. https://doi.org/10.1029/2000jd900719

Taylor KE, Stouffer RJ, Meehl GA (2012) An Overview of CMIP5 and the experiment design. Bull Am Meteorol Soc 93:485–498. https://doi.org/10.1175/bams-d-11-00094.1

Wang L, Chen W (2013) The East Asian winter monsoon: re-amplification in the mid-2000s. Chin Sci Bull 59:430–436. https://doi.org/10.1007/s11434-013-0029-0

Wang S, Chen W, Chen S, Nath D, Wang L (2019) Anomalous winter moisture transport associated with the recent surface warming over the Barents–Kara seas region since the mid-2000s. Int J Climatol. https://doi.org/10.1002/joc.6337

Warner J, Screen JA, Scaife AA (2019) Links Between Barents-Kara Sea Ice and the Extratropical Atmospheric Circulation Explained by Internal Variability and Tropical Forcing. Geophys Res Lett 47:1. https://doi.org/10.1029/2019GL085679

Xu M, Xu H, Jing M (2016) Responses of the East Asian winter monsoon to global warming in CMIP5 models. Int J Climatol 36:2139–2155. https://doi.org/10.1038/ncomms5646

Zhang P, Wu Y, Simpson IR, Smith KL, Zhang X, De B, Callaghan P (2018) A stratospheric pathway linking a colder Siberia to Barents–Kara Sea sea ice loss. Sci Adv 4:eaat6025. https://doi.org/10.1126/sciadv.aat6025

Zygmuntowska M, Mauritsen T, Quaas J, Kaleschke L (2012) Arctic clouds and surface radiation—a critical comparison of satellite retrievals and the ERA-Interim reanalysis. Atmos Chem Phys 12:6667–6677